Chinese Journal of Aeronautics, 2013,26(4): 1057–1063

Chinese Society of Aeronautics and Astronautics
& Beihang University

Chinese Journal of Aeronautics

cja@buaa.edu.cn
www.sciencedirect.com

Cutting force prediction for circular end milling process

Wu Baohai [a,*], Yan Xue [b], Luo Ming [a], Gao Ge [a]

[a] *Key Laboratory of Contemporary Design and Integrated Manufacturing Technology, Ministry of Education, Northwestern Polytechnical University, Xi'an 710072, China*
[b] *AVIC Commercial Aircraft Engine Co. Ltd., Shanghai 200241, China*

Received 12 April 2012; revised 8 June 2012; accepted 26 July 2012
Available online 28 April 2013

KEYWORDS

Chip thickness;
Circular end milling;
Cutting force;
Machining;
Radial depth;
Tool path curvature

Abstract A deduced cutting force prediction model for circular end milling process is presented in this paper. Traditional researches on cutting force model usually focus on linear milling process which does not meet other cutting conditions, especially for circular milling process. This paper presents an improved cutting force model for circular end milling process based on the typical linear milling force model. The curvature effects of tool path on chip thickness as well as entry and exit angles are analyzed, and the cutting force model of linear milling process is then corrected to fit circular end milling processes. Instantaneous cutting forces during circular end milling process are predicted according to the proposed model. The deduced cutting force model can be used for both linear and circular end milling processes. Finally, circular end milling experiments with constant and variable radial depth were carried out to verify the availability of the proposed method. Experiment results show that measured results and simulated results corresponds well with each other.

1. Introduction

End milling is widely used in machining moulds and dies, as well as various aircraft components. To ensure cutting quality, tool life prolongation and the productivity, accurate milling process analysis is critically necessary for beforehand process planning and adaptive controlling. During the entire milling process, cutting force is one of the most important issues and an efficient and precise cutting force model is thus crucial for the selection of machining parameters, such as feed rate, and spindle speed.

Traditional researches[1,2] on cutting force model usually focus on linear milling process. Chip thickness calculation[3–5] as well as cutting force coefficients identification[6–9] is also analyzed specially for linear milling force simulation. These approaches do not always meet other cutting conditions, especially circular milling process. In Refs. [10,11], cutting condition independent force coefficients concept was introduced into milling force modeling, however; precise instantaneous uncut chip thickness and runout offset and angle factors are needed in this method to get desirable instantaneous cutting force coefficients. Size effect and other characteristics during the process may influence the simulation results eventually. Therefore a particular model for circular milling is necessary to satisfy practical request.

Regarding force simulation of circular milling, relative researches have been done recently. Zhang et al.[12,13] proposed

* Corresponding author. Tel.: +86 29 88493232 414.
E-mail addresses: wubaohai@nwpu.edu.cn (B. Wu), yanxueyx@gmail.com (X. Yan), luoming@nwpu.edu.cn (M. Luo).

Peer review under responsibility of Editorial Committee of CJA.

Production and hosting by Elsevier

1000-9361 © 2013 Production and hosting by Elsevier Ltd. on behalf of CSAA & BUAA. Open access under CC BY-NC-ND license.
http://dx.doi.org/10.1016/j.cja.2013.04.003

an approach to predict the cutting forces in the end milling of rectangular circular corner profiles by discretizing the corner into a series of steady-state cutting processes, each with different radial depth of cut. Wu et al.[14] investigated the relationship between working parameters and the corner coordinates by way of combination of tool tracing and cutting geometrodynamics. Yang et al.[15] developed a method for cutting force modeling related to peripheral milling of curved surfaces including the effect of cutter runout. For curved surface milling process, Rao et al.[16–20] presented a series of accomplishment concluding process geometry, curvature effect, cutting force, surface error and so on.

Although the above-mentioned literature has extended to a bunch of stuff for circular milling, it does not mention the variation of feed rate along cutting tool envelope during circular milling process. For the existence of workpiece curvature, the feed rate along the cutting tool envelope will not remain the same as that of the tool center, and this is an important difference from the linear milling process. When establishing a cutting force model, one of the key issues is the calculation of instantaneous chip thickness, which has dependent relationship with feed rate. Abundant researches have been done on this aspect.[3,4,21] The effects of runout, tooth trajectory as well as tool deflection on chip thickness are discussed, respectively or simultaneously. It is noticed that studying the cutting force in milling with a circular tool path, the variation of uncut chip thickness is too important to be neglected. Actually the key elements involved in force model, for instance, feed rate and chip thickness, will deviate from their normal values during circular milling process.

This paper proposes a cutting force prediction model for circular end milling process by improving the chip thickness model. And this paper is organized as follows: a review of the related literature is presented in Section 1, followed by mechanics of circular milling process in Section 2. In Section 3, the method for identification of cutting force coefficients is proposed, followed by experimental validation and discussion in Section 4. Finally, conclusions are given in Section 5. For the sake of simplicity, the following assumptions are firstly made: end-milling process is assumed to be chatter-free. And the deflection of the cutter and workpiece are assumed to be negligible.

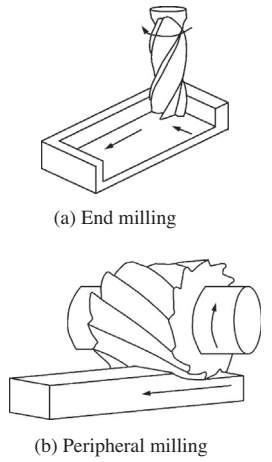

Fig. 1 End milling and peripheral milling.

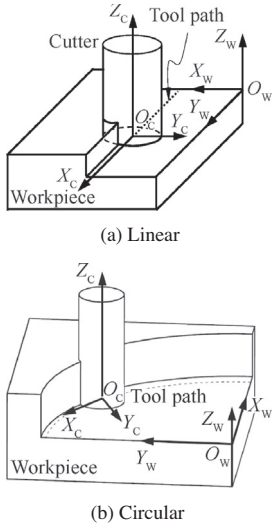

Fig. 2 Geometry of linear and circular end milling process.

2. Mechanics of circular end milling

As shown in Fig. 1, in the end milling process, the cutter generally rotates on an axis vertical to the workpiece. Cutting teeth are located on both the end face of the cutter and the periphery of the cutter body. The cutter can be tilted to machine tapered surfaces. While in peripheral milling, the axis of cutter rotation is parallel to the workpiece surface to be machined, and the cutter has a number of teeth along its circumference.

2.1. Geometry of circular end milling process

To analyze geometry of circular end milling process, a series of plane Cartesian coordinate systems is defined first. As shown in Fig. 2, a plane Cartesian coordinate system $O_W X_W Y_W Z_W$ is fixed on the workpiece. For circular milling process, coordinate origin O_W coincides with the arc center of finished workpiece, and the directions of X_W axis and Y_W axis depend on the cutting force measuring device. Coordinate system $O_C X_C Y_C Z_C$ is fixed with the cutter center and has a synchronous motion in $X_W Y_W$ plane corresponding to the motion of cutter along tool path. Its X_C axis is always oriented in the instantaneous feed direction, Y_C axis locates on the line of current cutter center and O_W of global coordinate, and Z_C axis coincides with the cutter axis.

As shown in Fig. 3, during linear milling process, if the tool path is straight line, then the feed rate of every cutting point along the cutter envelope keeps constant, and equals normal feed rate f, here f refers to the feed per tooth. But during circular milling process, the cutter center path is circular and the instant feed rate of the cutting point on the cutter is f when it is just located on the path, as shown in Fig. 3. In the figure, R refers to radius of tool path, r is the radius of the cutter, ϕ is the tool instantaneous angle position. The feed rates of other cutting points along the cutter envelope are relative to the radius of toolpath and the distance with cutter center.

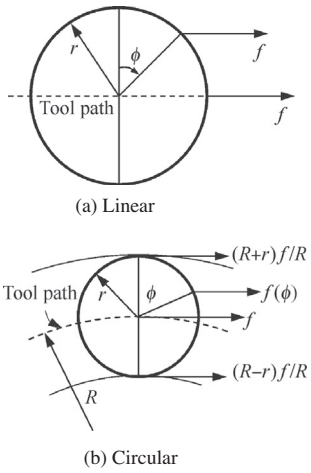

Fig. 3 Feedrate along cutter circum during linear and circular milling.

2.2. Cutting force model

The commonly used mechanistic model of cutting force model for milling process deduced by Altintas and Lee[1] is adopted here. To calculate the total force, the cutting flute is divided into finite number of small differential elements along the cutting flute curve, and the total cutting force components acting on a flute at a particular instant are obtained by numerically integrating the force components acting on an individual differential element.

The tangential force dF_T is in the direction of cutting speed. The radial force dF_R is in the radial direction of cutter feed, and the axial cutting force dF_A acts along the cutter axial direction.

$$\begin{cases} dF_{j,T}(\phi_j, z) = K_T h(\phi_j, z) db \\ dF_{j,R}(\phi_j, z) = K_R h(\phi_j, z) db \\ dF_{j,A}(\phi_j, z) = K_A h(\phi_j, z) db \end{cases} \quad (1)$$

where K_T, K_R and K_A are the tangential, radial and axial cutting force coefficients, $h(\phi_j, z)$ is the instantaneous chip thickness which is related to the cutting edge segment with a differential length of dz, and varies with the position of the cutting point and cutter's rotation. db is the projected length of an infinitesimal cutting flute in the direction along the cutting velocity, $\phi_j(z)$ is the instantaneous angular position of the jth tooth at axial elevation z, and it can be expressed as

$$\phi_j(z) = \phi_1(z) + (j-1)\phi_p \quad (2)$$

where $\phi_1(z)$ is the rotation angle of reference flute measured from positive direction of Y-axis, $\phi_p = 2\pi/N$ is the pitch angle and N is the number of cutter teeth.

Three orthogonal force components in Cartesian coordinates system of ith cutter element for jth tooth can be obtained by following transformation of the tangential, radial and axial forces defined on the cutting flute element:

$$\begin{bmatrix} dF_{i,j,X}(\phi_{i,j}, z) \\ dF_{i,j,Y}(\phi_{i,j}, z) \\ dF_{i,j,Z}(\phi_{i,j}, z) \end{bmatrix} = \boldsymbol{M} \begin{bmatrix} dF_{i,j,T} \\ dF_{i,j,R} \\ dF_{i,j,A} \end{bmatrix} \quad (3)$$

where

$$\boldsymbol{M} = \begin{bmatrix} -\cos\phi_{i,j} & -\sin\phi_{i,j} & 0 \\ \sin\phi_{i,j} & -\cos\phi_{i,j} & 0 \\ 0 & 0 & -1 \end{bmatrix}$$

Then the total force acting on the jth cutting edge can be obtained by integrating along the axial depth of cut:

$$F_{.j} = \int_{z_1}^{z_2} dF_{.j} dz \quad (4)$$

And z_1, z_2 depend on the immersion condition of jth tooth. Finally the total cutting forces on the milling cutter in feed (X), normal (Y) and axial (Z) directions are obtained by summing the contribution of all cutting edges.

$$F_{X,Y,Z} = \sum_{j=1}^{N_f} F_{.j} \quad (5)$$

2.3. Mechanics of circular end milling

Chip thicknesses for linear and circular end milling process are different. For linear milling process, chip thickness is determined as follows

$$\text{Model 1}: h(\phi) = f\sin(\phi)$$

where f is the normal feed per tooth, $\epsilon[0, \pi]$.

Then for circular end milling process, chip thickness could be expressed as

$$\text{Model 2}: h(\phi) = f(\phi)\sin(\phi) = f\sin(\phi)[R + r\cos(\phi)]/R$$

Fig. 4 shows the chip thickness (h) of circular end milling process under chip thickness Model 1 and Model 2. The results show that appearance of the maximum chip thickness corresponds to different tool rotation angles, and values of the maximum chip thickness are almost the same. It reveals the difference between the two models.

3. Identification of cutting force coefficients

Linear milling data are usually utilized for the identification of cutting force coefficients[1], and the same procedure is applied in this research. The cutting force coefficients are treated as constants that are calibrated based on equating the measured and analytical average cutting forces per tooth.

$$\overline{F}_{X,Y,Z} = \frac{1}{\phi_p} \int_{\phi_{st}}^{\phi_{ex}} \int_{z_1}^{z_2} dF_{X,Y,Z}(\phi, z) d\phi \quad (6)$$

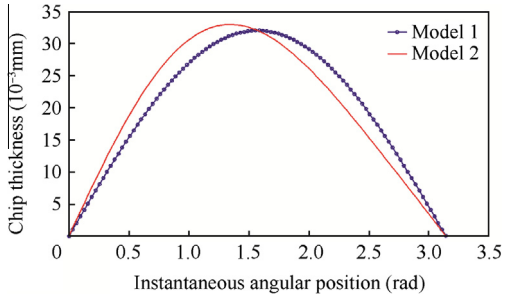

Fig. 4 Chip thickness of circular end milling with different models.

where ϕ_{st} and ϕ_{ex} denote the start and exit radial immersion angles, respectively. Especially for slot milling process, substituting $\phi_{st} = 0$ and $\phi_{ex} = \pi$ into Eq. (6), and following equations expressing the average cutting forces per tooth in the three directions can be obtained:

$$[F_X(\phi) \quad F_Y(\phi) \quad F_Z(\phi)]^{\mathrm{T}} = \frac{f_z}{2}\boldsymbol{\Psi}[A_1 \quad A_2 \quad A_3]^{\mathrm{T}} \tag{7}$$

where

$$\boldsymbol{\Psi} = \begin{bmatrix} -K_{\mathrm{T}}\sin(2\phi) & -2K_{\mathrm{R}}\sin^2\phi & -2K_{\mathrm{A}}\sin^2\phi \\ 2K_{\mathrm{T}}\sin^2\phi & -K_{\mathrm{R}}\sin(2\phi) & -K_{\mathrm{A}}\sin(2\phi) \\ 0 & -2K_{\mathrm{A}}\sin\phi & 2K_{\mathrm{R}}\sin\phi \end{bmatrix},$$

$$A_1 = \int_{z_1}^{z_2} \mathrm{d}z, \quad A_2 = \int_{z_1}^{z_2} \sin\kappa(z)\mathrm{d}z, \quad A_3 = \int_{z_1}^{z_2} \cos\kappa(z)\mathrm{d}z$$

$$[\overline{F}_X \quad \overline{F}_Y \quad \overline{F}_Z]^{\mathrm{T}} = \frac{f_z}{\phi_p}\boldsymbol{D}[K_{\mathrm{T}} \quad K_{\mathrm{R}} \quad K_{\mathrm{A}}]^{\mathrm{T}} \tag{8}$$

where

$$\boldsymbol{D} = \begin{bmatrix} C_3A_1 & (C_2-C_1)A_2 & (C_2-C_1)A_3 \\ -(C_2-C_1)A_1 & C_3A_2 & C_3A_3 \\ 0 & -C_4A_3 & C_4A_2 \end{bmatrix},$$

$$C_1 = \frac{1}{2}\phi\Big|_{\phi_{st}}^{\phi_{ex}}, \qquad C_2 = \frac{1}{4}\sin(2\phi)\Big|_{\phi_{st}}^{\phi_{ex}}$$

$$C_3 = \frac{1}{4}\cos(2\phi)\Big|_{\phi_{st}}^{\phi_{ex}}, \quad C_4 = \cos\phi\Big|_{\phi_{st}}^{\phi_{ex}}$$

Then the cutting force coefficients can be expressed as follows:

$$\begin{cases} K_{\mathrm{T}} = \frac{2\pi}{f_z N A_1}\frac{C_3\overline{F}_X-(C_2-C_1)\overline{F}_Y}{C_3^2+(C_2-C_1)^2} \\ K_{\mathrm{R}} = \varsigma\left\{\frac{A_2[(C_2-C_1)\overline{F}_X+C_3\overline{F}_Y]}{C_3^2+(C_2-C_1)^2} - \frac{A_3\overline{F}_Z}{C_4}\right\} \\ K_{\mathrm{A}} = \varsigma\left\{\frac{A_3[(C_2-C_1)\overline{F}_X+C_3\overline{F}_Y]}{C_3^2+(C_2-C_1)^2} + \frac{A_2\overline{F}_Z}{C_4}\right\} \end{cases} \tag{9}$$

where

$$\varsigma = \frac{2\pi}{f_z N(A_2^2 + A_3^2)}$$

4. Experimental validation and discussion

4.1. Cutting force data processing

During the practical milling process, cutting force can be affected by various factors, such as cutter runout, tool deflection and edge wear. In this paper, tool deflection and edge wear are not taken into consideration. Cutter runout is a common phenomenon in milling operations, and it affects the chip load distribution of every tooth. To remove the effects of cutter runout, the flute-average method[22] (FAM) is applied to the cutting force in this paper. In this method, sample points spaced by the flute-spacing angle are averaged over one revolution to obtain an average flute force profile. Fig. 5 shows the cutting forces before and after FAM.

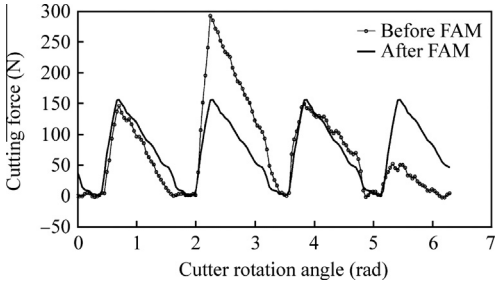

Fig. 5 Cutting force before and after FAM.

4.2. Identification of cutting force coefficients

Cutting forces were measured during full slot milling Titanium alloy TC4 at different feed rates. Tool geometrical parameters are listed in Table 1.

Table 1 Tool geometry.

Symbol	Terminology	Value
D_{T}	Tool diameter (mm)	10
H	Overhang length (mm)	38
L	Tool length (mm)	75
N	Number of teeth	4
β	Helix angle (°)	30

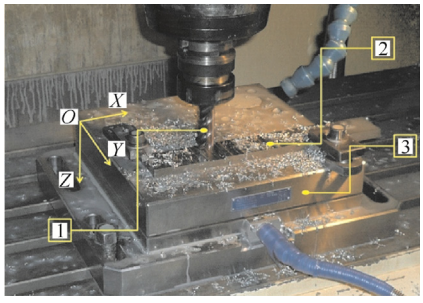

1—Cutter; 2—Workpiece; 3—Kistler 9255 B

Fig. 6 Experimental setup.

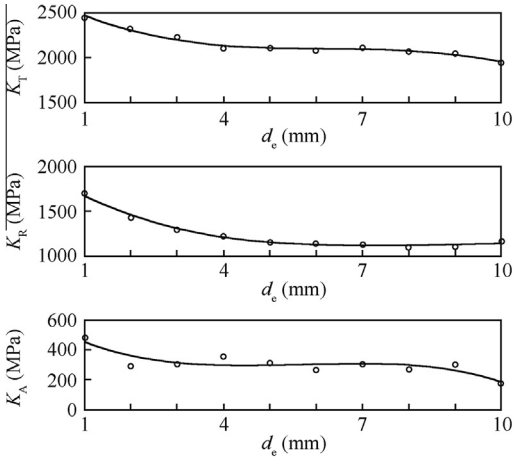

Fig. 7 Cutting force coefficients under different cutting conditions.

The axial depth of cut is kept constant at 2 mm, and the radial depth changes from 1 mm to 9 mm. The feedrate is 320 mm/min and the spindle speed is 2000 rpm. Cutting forces during the milling process were recorded with Kistler 9255B cutting force measuring device shown in Fig. 6.

Polynomial fitting method was then used for different radial depths of cut d_e, as shown in Fig. 7. The small circle in the figure represents the identified cutting force coefficients under different redial depth of cut.

With this method, the effects of different radial depth can be taken into account. Finally, the expressions of the cutting force coefficients are as follows:

$$\begin{cases} K_T = -2.92d_e^3 + 51.82d_e^2 - 309.3d_e + 2727 \\ K_R = -1.618d_e^3 + 39.85d_e^2 - 318.7d_e + 1947 \\ K_A = -2.055d_e^3 + 34.54d_e^2 - 183.0d_e + 603.5 \end{cases} \quad (10)$$

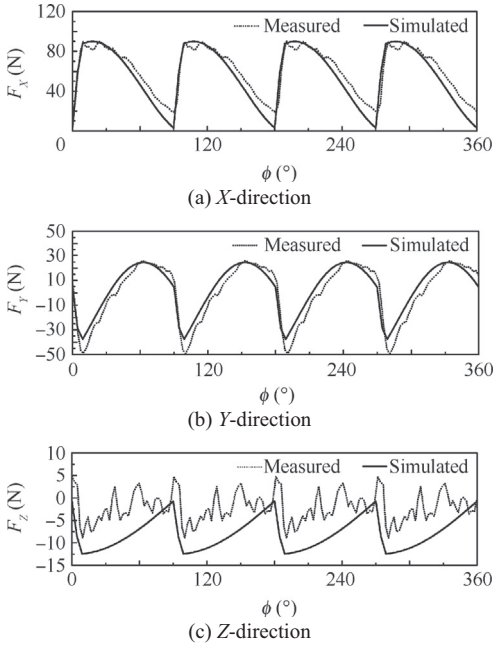

Fig. 8 Simulated and measured cutting force.

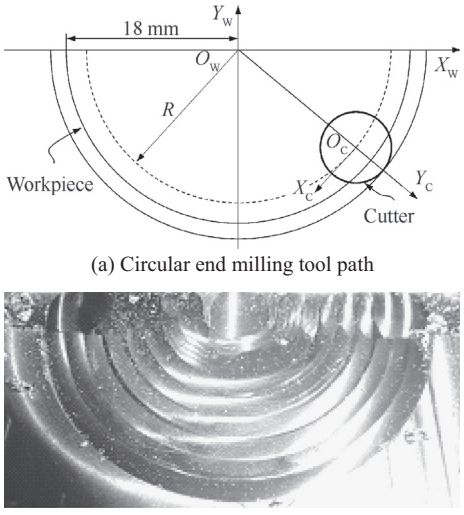

Fig. 9 Circular end milling tool path and machined workpiece.

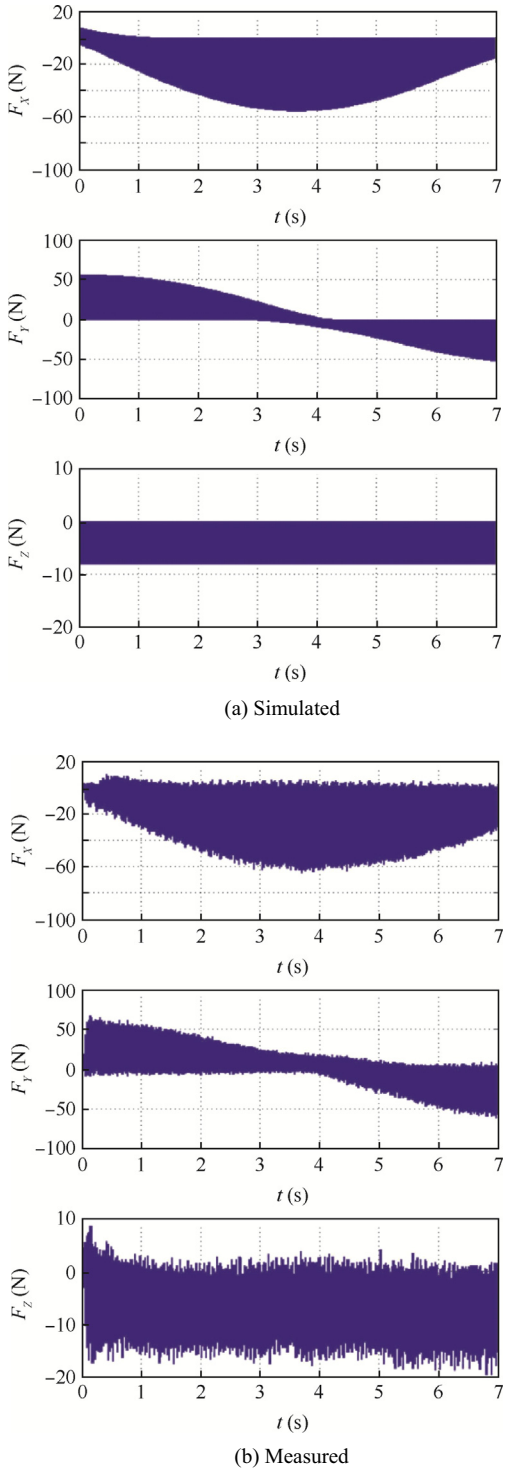

Fig. 10 Simulated and measured cutting forces for circular end milling with constant radial depth.

4.3. Cutting force simulation of linear milling

Cutting force simulation with the proposed method for linear milling process was carried out. The cutter and workpiece material used here are the same as the above. The spindle speed is 2000 rpm, federate is 320 mm/min, the radial cutting depth is 5 mm and 1 mm in axial cutting depth. As shown in Fig. 8, simulated results and measured results correspond well with each other.

4.4. Cutting force simulation of circular milling

4.4.1. Constant radial depth

To validate the effectiveness of the proposed method in circular milling process, experiments are carried out. For the first experiment, as shown in Fig. 9, the cutter follows the semicircular tool path with 18 mm in radius. The cutting tool used here is the same as above, cutting parameters are listed below: feedrate 320 mm/min, spindle speed 2500 rpm, axial depth 1 mm, tool path radius $R = 13$ mm, radial depth $d_e = 1$ mm.

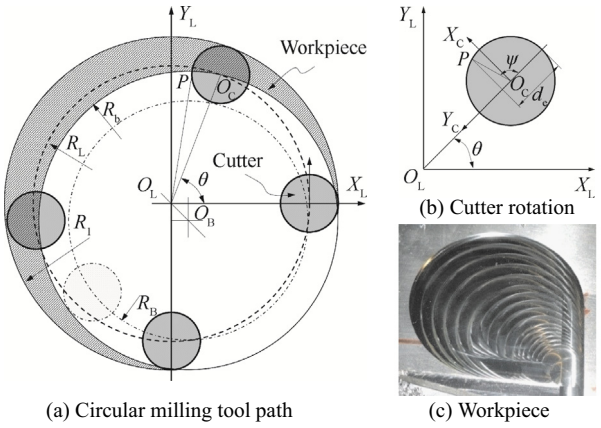

Fig. 11 Circular end milling with variable radial depth of cut.

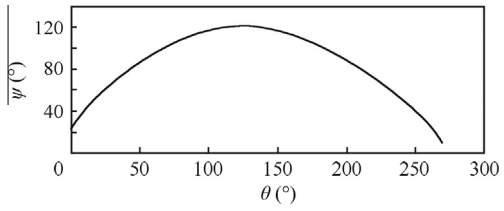

Fig. 12 Cutter-workpiece engagement angle variation.

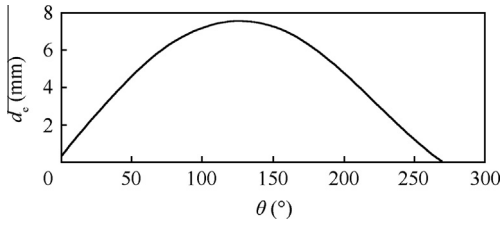

Fig. 13 Variation of radial depth of cut.

Simulated and measured cutting forces are shown in Fig. 10. Results show that simulated and measured values have the same profile, and the cutting force amplitude in both X- and Y-direction corresponds well with each other. Measured force amplitude in Z-direction is larger than simulated ones, and it is due to the inaccuracy in Z-direction of the measuring device.

4.4.2. Variable radial depth

As for circular milling with variable radial depth shown in Fig. 11, O_L is the center of current circular tool path, O_B is

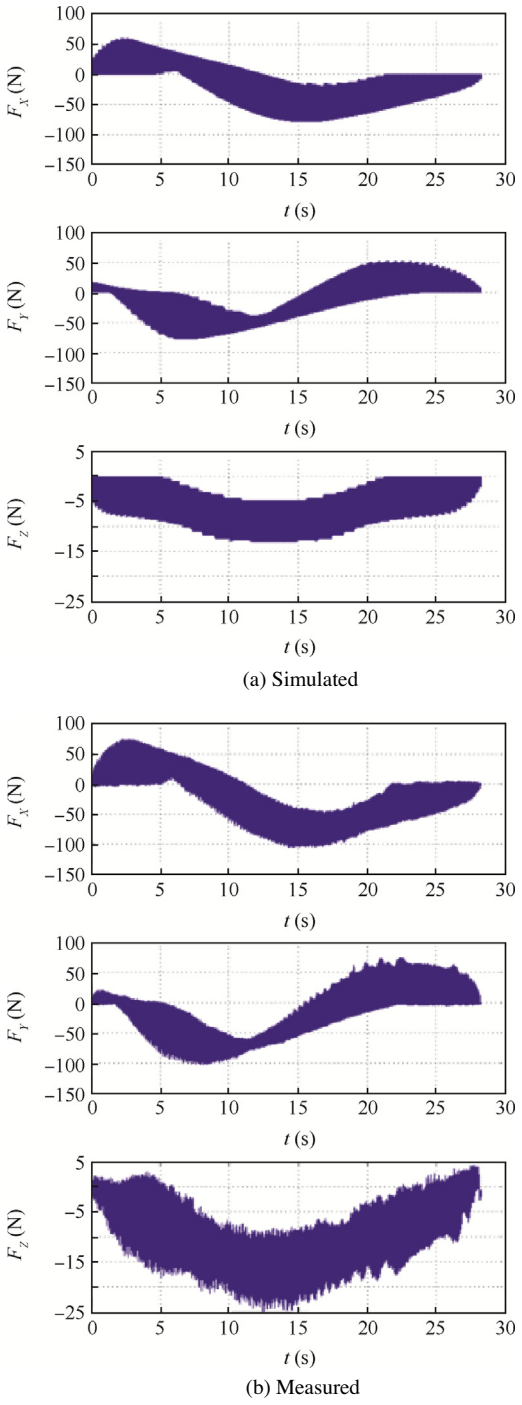

Fig. 14 Simulated and measured cutting forces for circular milling with variable radial depth.

the center of previous circular tool path, O_C is the center of the cutter, R_L is the radius of current tool path, R_B is the radius of previous tool path, R_b is the radius of current machined surface, R_l is the radius after machining, P is the intersection point between the cutter profile and the machined surface, ψ is tool immersion angle, θ is cutter position angle regard to the X_L direction of current circular tool path. While following the specific tool path, the instantaneous cutter-workpiece engagement angle of the cutter is shown in Fig. 12, and the radial depth variation is shown in Fig. 13.

Simulated and measured cutting forces in three directions are shown in Fig. 14. In the experiment, radius of the previous tool path is 29 mm, and 32 mm for current tool path. Radius of the workpiece profile before milling is 34 mm, and 37 mm after milling.

Results show that both cutting force profile and amplitude in X and Y directions correspond well. Cutting force in Z direction of simulated ones and measured ones has the same profile, but the amplitude is much larger than that of measured ones, which is due to the inaccuracy and zero elegant in Z direction of the measuring device.

5. Conclusions

A cutting force prediction model considering the tool path curvature for circular end milling process is studied in this paper. Validation of the proposed method has been demonstrated through a serious of milling experiments. The main contributions of this paper are listed as follows:

(1) By taking tool path curvature into account the chip thickness model has been improved for circular end milling process.
(2) With the improved chip thickness model, cutting force model for circular end milling process has been deduced and the simulation results meet the measured results well.
(3) The deduced cutting force model can be used not only for linear and circular end milling processes, but also for freeform splines if improved.

Acknowledgements

This study was co-supported by Open National Natural Science Foundation of China (No. 51005183), National Science and Technology Major Project (No. 2011ZX04016031) and China Postdoctoral Science Foundation (No. 2012M521804).

References

1. Altinta Y, Lee P. A general mechanics and dynamics model for helical end mills. *CIRP Ann Manuf Technol* 1996;**45**(1):59–64.
2. Kline WA, Devor RE. The effect of runout on cutting geometry and forces in end milling. *Int J Mach Tool Des Res* 1983;**23**(2–3):123–40.
3. Spiewak S. An improved model of the chip thickness in milling. *CIRP Ann Manuf Technol* 1995;**44**(1):39–42.
4. Li HZ, Liu K, Li XP. A new method for determining the undeformed chip thickness in milling. *J Mater Process Technol* 2001;**113**(1–3):378–84.
5. Kumanchik LM, Schmitz TL. Improved analytical chip thickness model for milling. *Precision Eng* 2007;**31**(3):317–24.
6. Budak E, Altintas Y, Armarego EJA. Prediction of milling force coefficients from orthogonal cutting data. *J Manuf Sci Eng* 1996;**118**(2):216–24.
7. Gradišek J, Kalveram M, Weinert K. Mechanistic identification of specific force coefficients for a general end mill. *Int J Mach Tools Manuf* 2004;**44**(4):401–14.
8. Wan M, Zhang WH, Qin GH, Tan G. Efficient calibration of instantaneous cutting force coefficients and runout parameters for general end mills. *Int J Mach Tools Manuf* 2007;**47**(11):1767–76.
9. Gonzalo O, Beristain J, Jauregi H, Sanz C. A method for the identification of the specific force coefficients for mechanistic milling simulation. *Int J Mach Tools Manuf* 2010;**50**(9):765–74.
10. Yun WS, Cho DW. Accurate 3-D cutting force prediction using cutting condition independent coefficients in end milling. *Int J Mach Tools Manuf* 2001;**41**(4):463–78.
11. Ko JH, Cho DW. Determination of cutting-condition-independent coefficients and runout parameters in ball-end milling. *Int J Adv Manuf Technol* 2005;**26**(11):1211–21.
12. Zhang L, Zheng L. Prediction of cutting forces in milling of circular corner profiles. *Int J Mach Tools Manuf* 2004;**44**(2–3):225–35.
13. Zhang L, Zheng L. Prediction of cutting forces in end milling of pockets. *Int J Adv Manuf Technol* 2005;**25**(3):281–7.
14. Wu Q, Zhang YD, Zhang HW. Corner milling of thin walled cavities on aeronautical components. *Chin J Aeronaut* 2009;**22**(6):677–84.
15. Yang Y, Zhang WH, Wan M. Effect of cutter runout on process geometry and forces in peripheral milling of curved surfaces with variable curvature. *Int J Mach Tools Manuf* 2011;**51**(5):420–7.
16. Rao VS, Rao PVM. Modelling of tooth trajectory and process geometry in peripheral milling of curved surfaces. *Int J Mach Tools Manuf* 2005;**45**(6):617–30.
17. Rao VS, Rao PVM. Effect of workpiece curvature on cutting forces and surface error in peripheral milling. *J Eng Manuf* 2006;**220**(9):1399–407.
18. Rao VS, Rao PVM. Tool deflection compensation in peripheral milling of curved geometries. *Int J Mach Tools Manuf* 2006;**46**(15):2036–43.
19. Desai KA, Rao PVM. Effect of direction of parameterization on cutting forces and surface error in machining curved geometries. *Int J Mach Tools Manuf* 2008;**48**(2):249–59.
20. Desai KA, Agarwal PK, Rao PVM. Process geometry modeling with cutter runout for milling of curved surfaces. *Int J Mach Tools Manuf* 2009;**49**(12–13):1015–28.
21. Sa L, Bouzid W, Zghal A. Chip thickness analysis for different tool motions: for adaptive feed rate. *J Mater Process Technol* 2008;**204**(1–3):213–20.
22. Yang L. Identification of depth-of-cut variations and their effects on the process monitoring for the end milling process dissertation. Illinois: University of Illinois at Urbana-Champaign; 2005.

Wu Baohai received his Ph.D. degrees Xi'an Jiaotong University in 2005. He is now an associate professor of Northwestern Polytechnical University. His main research interests are multi-axis machining and smart machining.

Yan Xue received her Ph.D. degree from Northwestern Polytechnical University in 2012. She is now an engineer of AVIC commercial aircraft engine CO.LTD.

Luo Ming received his Ph.D. degree from Northwestern Polytechnical University in 2012. He is now an assistant research fellow of Northwestern Polytechnical University. His main research interests are multi-axis machining and machining dynamics.